ADVANCES IN ATMOSPHERIC SCIENCES, VOL. 35, JULY 2018, 796–812

• **Original Paper** •

An Asymmetric Spatiotemporal Connection between the Euro-Atlantic Blocking within the NAO Life Cycle and European Climates

Yao YAO* and Dehai LUO

Key Laboratory of Regional Climate-Environment for Temperate East Asia, Institute of Atmospheric Physics, Chinese Academy of Sciences, Beijing 100029*, China*

(Received 19 May 2017; revised 30 November 2017; accepted 19 December 2017)

ABSTRACT

This paper examines an asymmetric spatiotemporal connection and climatic impact between the winter atmospheric blocking activity in the Euro-Atlantic sector and the life cycle of the North Atlantic Oscillation (NAO) during the period 1950–2012. Results show that, for positive NAO (NAO^+) events, the instantaneous blocking (IB) frequency exhibits an enhancement along the southwest–northeast (SW–NE) direction from the eastern Atlantic to northeastern Europe (SW–NE pattern, hereafter), which is particularly evident during the NAO^+ decaying stage. By contrast, for negative NAO (NAO^-) events, the IB frequency exhibits a spatially asymmetric southeast–northwest (SE–NW) distribution from central Europe to the North Atlantic and Greenland (SE–NW pattern, hereafter). Moreover, for NAO^- (NAO^+) events, the most marked decrease (increase) in the surface air temperature (SAT) in winter over northern Europe is in the decaying stage. For NAO^+ events, the dominant positive temperature and precipitation anomalies exhibit the SW–NE-oriented distribution from western to northeastern Europe, which is parallel to the NAO^+-related blocking frequency distribution. For NAO^- events, the dominant negative temperature anomaly is in northern and central Europe, whereas the dominant positive precipitation anomaly is distributed over southern Europe along the SW–NE direction. In addition, the downward infrared radiation controlled by the NAO's circulation plays a crucial role in the SAT anomaly distribution. It is further shown that the NAO's phase can act as an asymmetric impact on the European climate through producing this asymmetric spatiotemporal connection with the Euro-Atlantic IB frequency.

Key words: North Atlantic Oscillation, blocking, temperature, precipitation, asymmetry

Citation: Yao, Y., and D. H. Luo, 2018: An asymmetric spatiotemporal connection between the Euro-Atlantic blocking within the NAO life cycle and European climates. *Adv. Atmos. Sci.*, **35**(7), 796–812, https://doi.org/10.1007/s00376-017-7128-9.

1. Introduction

The North Atlantic Oscillation (NAO) is an important low-frequency mode of climate variability in the form of a north–south seesaw pattern of pressure between the Azores and Iceland in the Northern Hemisphere (NH) (Walker and Bliss, 1932; Hurrell et al., 2003). Research on the variability and impacts of this mode has attracted considerable attention among atmospheric scientists because of its significant impacts on climate and weather in the Atlantic sector and its adjacent regions (Hurrell, 1995; Scaife et al., 2008).

In recent decades, extreme weather events (temperature, precipitation and wind) have been emerging more frequently under the warming climate (Cattiaux et al., 2010; Simolo et al., 2011), with numerous studies investigating their physical processes (e.g., Kenyon and Hegerl, 2008, 2010; Scaife et al., 2008). It has been recognized that the occurrence of extreme temperature events over Europe is related to large-scale circulation patterns such as the NAO and blocking events (Hurrell, 1995; Alexander et al., 2006; Scaife et al., 2008; Sillmann and Croci-Maspoli, 2009; Cattiaux et al., 2010; Wang et al., 2010; Ouzean et al., 2011; Gong and Luo, 2017). In particular, extreme cold temperatures in winter over Europe are closely associated with the blocking activity in the Euro-Atlantic sector (Sillmann et al., 2011). Buehler et al. (2011) found that winters with an increased number of blocking events are associated with negative temperature anomalies over central to eastern Europe and dryer conditions, whereas southern Europe experiences warmer and wetter conditions during such episodes. Pfahl and Wernli (2012) showed that, over large parts of the continental high-latitudes, warm temperature extremes often occur simultaneously with atmospheric blocking at the same location, while cold extremes are unassociated with atmospheric blocking at the same location. This hints that there is an asym-

* Corresponding author: Yao YAO
Email: yaoyao@tea.ac.cn

metric impact of atmospheric blocking on warm and cold extremes.

A link between the phase of the NAO and blocking events in the Euro-Atlantic sector has been established in previous studies (Shabbar et al., 2001; Luo, 2005a; Croci-Maspoli et al., 2007; Luo et al., 2007; Woollings et al., 2008). It has been revealed that, for positive NAO (NAO^+) events, there is a reduced blocking frequency over the North Atlantic and an enhanced blocking frequency over Europe, and the opposite for negative NAO (NAO^-) events (Scherrer et al., 2006; Croci-Maspoli et al., 2007; Luo et al., 2007; Woollings et al., 2008). In recent years, many investigators (Pelly and Hoskins, 2003; Benedict et al., 2004; Berrisford et al., 2007; Rivière and Orlanski, 2007; Strong and Magnusdottir, 2008; Woollings et al., 2008, 2010a) have connected blocking and NAO events to Rossby wave breaking (RWB), defined as the reversal of the potential temperature gradient at the tropopause level (McIntyre and Palmer, 1983). Benedict et al. (2004) suggested that the two phases of the NAO result from a succession of cyclonic and anticyclonic RWB events, which has also been confirmed by numerical experiments (Franzke et al., 2004). Luo (2005b) and Luo et al. (2007, 2014) used a nonlinear multi-scale interaction model to demonstrate that blocking and NAO events mainly arise from the evolution of pre-existing synoptic-scale eddies, which can be seen as the initial condition. In addition, deformed eddies are important for the maintenance of dipolar mode variation, as indicated by Nie et al. (2014, 2016). To some extent, NAO^- events and blocking over the North Atlantic are two sides of the same coin (Luo et al., 2007; Woollings et al., 2010a). More recently, Davini et al. (2012a) found that the variability of the NAO pattern and its recent eastward shift are closely related to changes in the frequency of the Greenland blocking (GB). In years with high GB frequency the NAO pattern is in a negative phase and shifted westward, but in years with low GB frequency the first EOF of the Euro-Atlantic sector undergoes an eastward shift and looks more like the East-Atlantic pattern.

Although the phase of the NAO affects the frequency distribution of blocking events over the Atlantic and Europe (Shabbar et al., 2001; Croci-Maspoli et al., 2007), it is, however, unclear how the blocking frequency distribution changes during different stages (such as the growing stage or decaying stage) of the NAO life cycle. In particular, it is unclear how temperature and precipitation anomalies change during the different stages of the NAO and are linked with the blocking frequency distribution. Thus, the present study focuses on which stage of the NAO's life cycle the temperature and precipitation may change the most and is the nature of their spatial distribution. We also seek to uncover the physical mechanism or processes behind these changes. The investigation of these unsolved issues is a complement to previous studies and will help us understand the underlying physical processes of the NAO and blocking, and how they regulate regional weather and climate change on the sub-weekly scale, which may be of significance to the weekly prediction of temperature and precipitation.

Following this introduction, section 2 describes the data and methodology. Section 3 presents the results on the relationship between the blocking activity in the Euro-Atlantic region and the different phases of NAO events during their life cycles. The evolution of surface air temperature (SAT) and precipitation anomalies and their linkages to the phase of the NAO are examined in section 4. We further explore the relationship of the temperature and precipitation anomaly changes with the blocking frequency distribution for the different phases of the NAO in section 5. A physical explanation for why the spatial distribution of the blocking frequency is controlled by the phase of the NAO is provided in section 6. Conclusions and discussion are provided in the final section.

2. Data and method

2.1. *Data*

The data used in this study include the daily 500-hPa geopotential height fields on a $2.5^\circ \times 2.5^\circ$ grid from the National Centers for Environmental Prediction–National Center for Atmospheric Research (NCEP–NCAR) during the period November 1950 to March 2012. The daily precipitation and temperature data over Europe are from European Climate Assessment & Dataset project (E-OBS gridded dataset), with a $0.5^\circ \times 0.5^\circ$ grid resolution, from November 1950 to March 2012 (Haylock et al., 2008). The normalized daily NAO index is from the NOAA/Climate Prediction Center (http://www.cpc.noaa.gov/) (Barnston and Livezey, 1987). In this study, the winter season is defined as a time interval of five months from November to March (NDJFM). We define the daily temperature or precipitation anomaly as the deviation of the daily temperature or precipitation from its winter-mean value during 1950–2012. The seasonal cycle has been removed in all the anomaly fields.

2.2. *Classification of NAO events*

An NAO^+ (NAO^-) event is defined to have taken place if the normalized daily NAO index is greater (less) than or equal to a standard deviation of +1.0 (−1.0) persisting for at least three consecutive days. NAO events can be categorized into two types: in-situ events and transition events, as defined in Luo et al. (2012). In-situ NAO events are events of one phase that are not preceded by the opposite phase. Transition events include NAO^+ and NAO^- events simultaneously. In this study, to keep the length of the paper to a minimum and because of the complexity of the relationship, transition NAO events are not considered. Accordingly, hereafter, NAO^+ and NAO^- events correspond to in-situ NAO^+ and in-situ NAO^-, respectively.

According to the classification of NAO events, it is possible to investigate how the NAO's variability affects the spatiotemporal change of the blocking frequency, and examine its effect on the evolutions of temperature and precipitation anomalies.

2.3. *Blocking index*

It is useful to use a blocking index to identify the blocking activity in the Euro-Atlantic sector during the different stages of NAO events and examine how the variability of temperature and precipitation anomalies over continental Europe depends upon the blocking frequency distribution. Many blocking indices have been developed to explore the blocking activity in the NH (Tibaldi and Molteni, 1990; Pelly and Hoskins, 2003; Diao et al., 2006; Scherrer et al., 2006). The two dimensional (2D) blocking index developed more recently by Davini et al. (2012b) is a useful tool for the identification of blocking activity because it can better capture the dynamics of a blocking flow and its 2D distribution. The 2D blocking index of Davini et al. (2012b) is an extension of the one-dimensional blocking index of Tibaldi and Molteni (1990), based on the daily 500-hPa geopotential height at each grid point. A similar 2D index was also proposed by Schwierz et al. (2004) and Scherrer et al. (2006) in terms of the potential vorticity field. The main results are consistent, although the mathematical expressions of these 2D indices are different (Davini et al., 2012a, 2012b). Here, the 2D index of Davini et al. (2012b) is exploited to detect the blocking activity in the Euro-Atlantic sector. To identify instantaneous blocking (IB), the meridional gradient reversal of the 500-hPa geopotential height (unit: m) is defined in a way similar to that in Davini et al. (2012b):

$$\mathrm{GHGS}(\lambda_0,\phi_0) = \frac{Z(\lambda_0,\phi_0) - Z(\lambda_0,\phi_S)}{\phi_0 - \phi_S}\ ; \tag{1a}$$

$$\mathrm{GHGN}(\lambda_0,\phi_0) = \frac{Z(\lambda_0,\phi_N) - Z(\lambda_0,\phi_0)}{\phi_N - \phi_0}\ ; \tag{1b}$$

$$\mathrm{GHGS}(\lambda_0,\phi_0) > 0\ , \quad \mathrm{GHGN}(\lambda_0,\phi_0) < 10\ ; \tag{1c}$$

$$\mathrm{GHGS}_2(\lambda_0,\phi_0) = \frac{Z_{500}(\lambda_0,\phi_S) - Z_{500}(\lambda_0,\phi_S - 15)}{15} < -5\ ; \tag{1d}$$

where $Z(\lambda_0,\phi_0)$ is the daily 500-hPa geopotential height at the grid point (λ_0,ϕ_0); $\lambda_0(\phi_0)$ is the grid-point longitude (latitude), which ranges from 0° to 360° (30°N to 75°N); $\phi_N = \phi_0 + 15$; and $\phi_S = \phi_0 - 15$.

An IB event is identified if Eq. (1c) is satisfied. According to Davini et al. (2012b), a single blocking event is defined if the large-scale blocking is occurring in a box of 5° latitude ×10° longitude, centered on that point for at least five days. However, it is important to note that, in this study, the NAO is the main body and all the analysis is based on the division of NAO events, including the NAO's phases and sub-periods, which are introduced below. Thus, in this study, the blocking frequency associated with the NAO is the IB frequency at each grid on each day, rather than a single blocking event with a large-scale scope and certain life cycle. The 2D blocking index can be used to obtain the spatial distribution of the IB frequency on each day in the Euro-Atlantic sector. Here, the IB frequency is expressed as the percentage of days in winter that are blocked. Very low-latitude blocking frequency in the Atlantic basin is excluded if the constraint given by Eq. (1d) is used (Davini et al., 2012b).

3. Relationship between blocking activity and NAO events during the NAO life cycle

3.1. *Climatological distribution of Euro-Atlantic blocking events*

It is useful to look at the climatological distribution of Euro-Atlantic blocking event frequency before examining the impact of NAO events on the blocking activity in the Euro-Atlantic sector. Figure 1a shows the winter (NDJFM) mean distribution of the IB frequency in the Euro-Atlantic sector during 1950–2012 in light of the 2D blocking index of Davini et al. (2012a). It is clear that the climatological blocking frequency distribution is characterized by two main blocking frequency maximums, over Greenland and the region from the eastern North Atlantic to western Europe. This result is consistent with the findings of Davini et al. (2012b), Luo et al. (2015a) and Scherrer et al. (2006), who used an absolute geopotential height (AGP) index. Moreover, there is another relatively small blocking frequency center in the Urals region (around 60°E), where the Urals blocking can play an important role in regulating the climate of East Asia (Luo et al., 2017; Yao et al., 2017). In the work of Scherrer et al. (2006), the location of the blocking frequency region over continental Europe tended to be at high latitudes, whereas in Davini et al. (2012b) the maximum frequency region for European blocking events was mainly at relatively lower latitudes (eastern North Atlantic and western Europe). In the present paper, we examine in detail how the blocking frequency distribution changes during the different stages within the NAO life cycle and how it affects the spatiotemporal evolutions of the SAT and precipitation anomalies.

3.2. *Composites of daily NAO indices*

To see how NAO events affect the variability of Euro-Atlantic blocking events, we first show a composite of daily NAO indices for in-situ NAO^+ and NAO^- events (Figs. 1b and c), corresponding to the identified NAO events as listed in Table 1. Here, lag(0) denotes the day with the strongest amplitude for in-situ NAO events. To clearly see how the temperature and precipitation anomalies evolve during the different NAO stages, it is useful to subdivide the life cycle of in-situ NAO events from lag(−10) to lag(10) days into four stages: B1 (from the beginning to the growing stage), from lag(−10) to lag(−5); B2 (growing stage), from lag(−5) to lag(0) [note: "B" means before lag(0)]; A1 (decaying stage), from lag(0) to lag(5); and A2 (from the decaying stage to the end), from lag(5) to lag(10) [note: "A" means after lag(0)]. Based on this division, we can analyze the SAT and precipitation variability in different stages of the NAO and its relationship with the IB frequency. It is hoped that the results

Table 1. Number of NAO events and days in winter 1950–2012.

	Number of events	Number of days
In-situ NAO^+	97	1688
In-situ NAO^-	99	1547

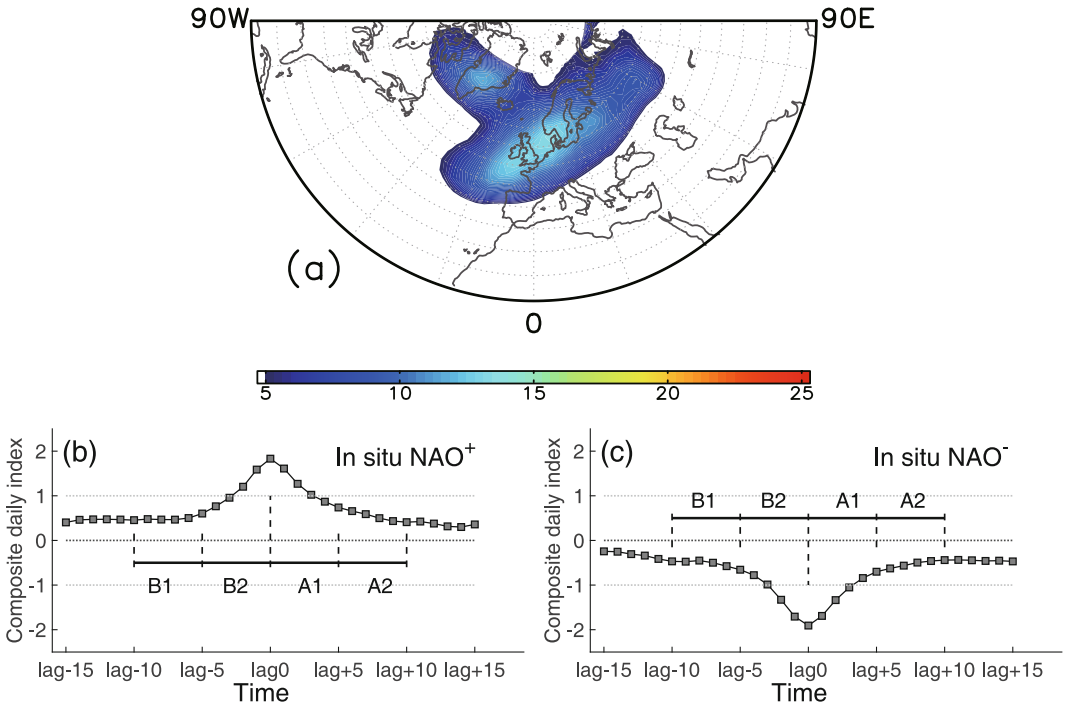

Fig. 1. (a) Geographical distribution of the climatological winter IB frequency during the winter period (ND-JFM) from 1950 to 2012. Shading is representative of the percentage of IB days with respect to the total days of a winter. The lines of latitude are plotted at 5° intervals starting at 20°N. Units: %. (b, c) Composite normalized daily NAO indices in winter for (b) in-situ NAO^+ and (c) in-situ NAO^- events during winter 1950–2012. B1, B2, A1 and A2 represent four sub-periods of the NAO life cycle. B (A) means before (after) the peak day lag(0).

obtained in this study can be used as a reference for climate prediction.

From Figs. 1b and c, the decaying of the in-situ NAO event seems slower than its growing stage. This may be related to persistent RWB during the decaying stage (Woollings et al., 2008). To see how NAO events modulate the blocking frequency, composites of the blocking frequencies for different types of NAO events are produced in terms of the composite daily NAO indices in the next subsection.

3.3. *Evolution of the blocking frequency distribution during the life cycle of NAO events*

In this subsection we examine how the phases of the NAO affect the frequency and location of Euro-Atlantic blocking, especially during the different stages within the NAO life cycle. In addition, as mentioned above, we use the IB frequency instead of blocking events. This is because, for a single NAO event, a blocking event within the life cycle of an NAO event cannot be separated into parts based on the NAO's four sub-periods. Also, in general, the occurrence of the NAO and blocking is always temporally uncertain, sometimes overlapping and sometimes leading or lagging. Thus, it seems reasonable to calculate the spatial distribution of the IB frequency in the different stages of the composite NAO event because the frequency of the IB has almost the same distribution pattern as that of the blocking events (Davini et al., 2012b; Luo et al., 2015a, 2015b; Yao and Luo, 2015). We show the spatial distribution of the composite IB frequency for the different stages of NAO^+ and NAO^- events in Fig. 2 in terms of the percentage of IB days with respect to total NAO days within each stage, as shown in Figs. 1b and c. As can be seen from Fig. 2a, for the NAO^+ events the higher blocking frequency is distributed like a tongue along the southwest–northeast (SW–NE) direction from the eastern Atlantic to northeastern Europe (Fig. 2a). Hereafter, the IB frequency distribution is referred to as the "SW–NE" pattern and its maximum frequency region varies with the different stages of the composite in-situ NAO^+ events. For example, the maximum frequency region seems to be uniformly distributed in western and central Europe during B2, but becomes mainly concentrated in the eastern Atlantic and western Europe during A1. For the composite blocking frequency of in-situ NAO^- events, the IB frequency distribution looks like a tongue along the southeast–northwest (SE–NW) direction from western Europe to Greenland during the period from B2 to A2 (Fig. 2b). Hereafter, such a blocking frequency distribution is referred to as the "SE–NW" pattern. During B1 the high blocking frequency is primarily located over western Europe, but is distributed along the SE–NW direction with two blocking frequency maximum regions, over Greenland and western Europe respectively, during B2. In particular, during A1 the blocking frequency maximum region tends to be concentrated in Greenland. Thus, the phase of the NAO not only affects the longitudinal location of the higher IB frequency over continental Europe, but also its latitudinal position.

By using the AGP index Scherrer et al. (2006) noted that for NAO$^-$ there is a significantly higher blocking frequency maximum over the Davis Strait, southern Greenland and the Norwegian Sea, while the NAO$^+$-related blocking frequency is mainly concentrated in the eastern Atlantic, central and western Europe (their Fig. 3). Through analysis of blocking tracks, Croci-Maspoli et al. (2007) found that the northwestern Atlantic exhibits significantly higher (lower)

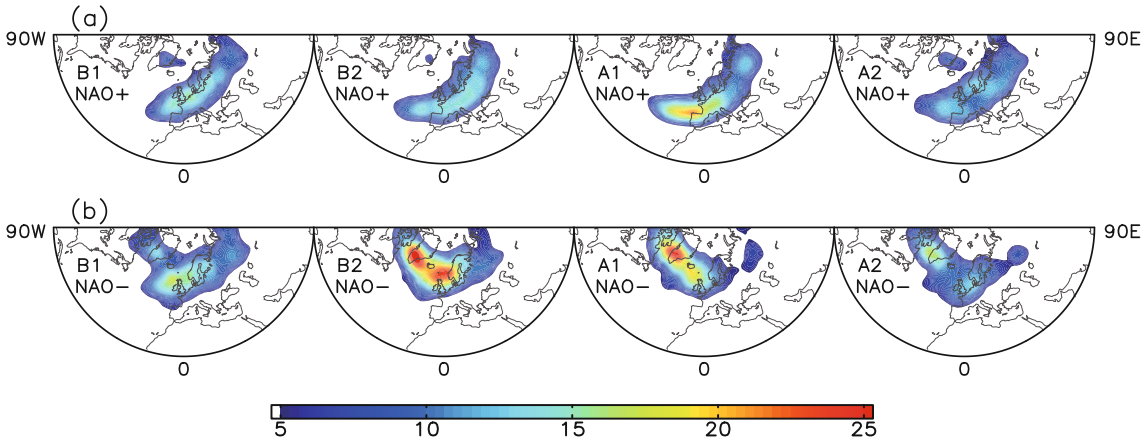

Fig. 2. Geographical distribution of IB frequencies in winter averaged for four sub-periods of NAO events: (a) NAO$^+$ events; (b) NAO$^-$ events. Shading is representative of the percentage of IB days with respect to total NAO days within each stage. The lines of latitude are plotted at 5° intervals starting at 20°N. Units: %.

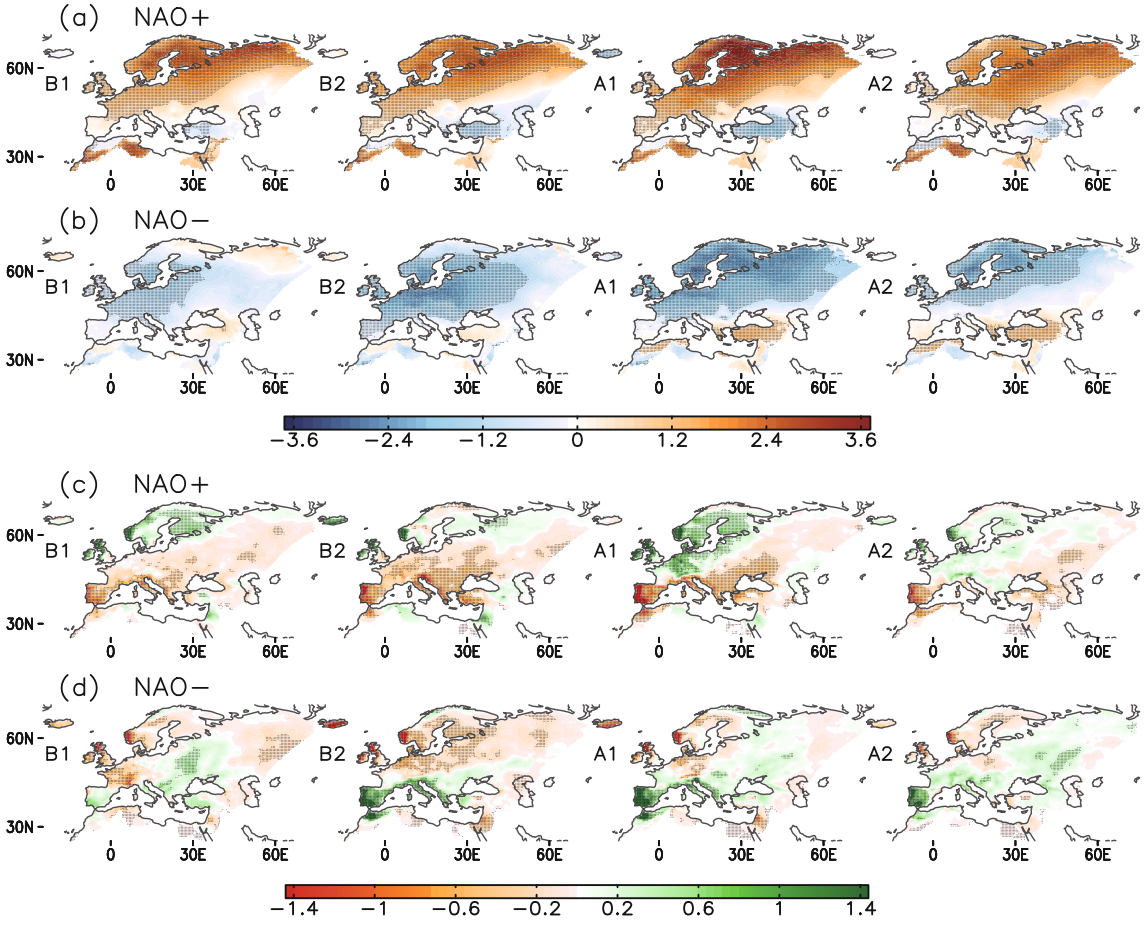

Fig. 3. Geographical distribution of composite surface (a, b) temperature and (c, d) precipitation anomalies in winter averaged for four sub-periods of NAO events: (a, c) NAO$^+$ events; (b, d) NAO$^-$ events. The stippling in all panels denotes positive (negative) anomaly values above the 95% confidence level for a two-sided Student's *t*-test. Units: °C in (a, b) and mm in (c, d).

blocking frequencies during NAO^- (NAO^+) events. In particular, during NAO^- events, blocking genesis occurs in a broad region extending from Newfoundland to the west coast of Greenland, but in the NAO^+ phase northeastward movement is evident for blocking genesis, such that many blockings reside in central Europe (Luo et al., 2007). The findings of Croci-Maspoli et al. (2007, see their Fig. 6a) show that there is a lower blocking frequency over continental Europe during NAO^- events. However, our result indicates a clear higher blocking frequency over northern and western Europe (Fig. 2b). The higher blocking frequency distribution reflects that NAO^- events originate from the retrogression of blocking events over northern Europe (Luo et al., 2007; Sung et al., 2011; Yao and Luo, 2015). Such a feature cannot be seen from the results of Croci-Maspoli et al. (2007). Woollings et al. (2008, Fig. 2) used a wave breaking index to find that in the Euro-Atlantic sector there are two maximum blocking frequency regions, over Europe and Baffin Island. For NAO^- events, the blocking frequency is enhanced over Greenland but reduced over southern Europe, with the opposite for NAO^- events. Recently, Mitchell et al. (2013) found that, under a strong Northern Annular Mode (NAM), the higher blocking frequency occurs in the mid-Atlantic and western Europe, whereas under a weak NAN it is over Baffin Island and Greenland. Although the blocking pattern presented here is similar to the results of Luo et al. (2015a), we further find that the spatial position of the maximum IB frequency depends on the different stages of the life cycle of NAO events. For example, for NAO^+ (NAO^-) events, the maximum IB frequency is centralized in the region from the eastern Atlantic and western Europe to northeastern Europe (Greenland to western Europe) during its growing stage, B2, but in the eastern Atlantic (Greenland) during its decaying stage, A1. This result is new and supplements the previous findings of Shabbar et al. (2001), Scherrer et al. (2006), Croci-Maspoli et al. (2007), Luo et al. (2015a) and Mitchell et al. (2013). Moreover, Fig. 2 also gives a quantitative analysis of the IB frequency during the NAO life cycle. The percentage of the IB frequency can account for more than 25% with respect to the B2 and A1 stages of the NAO, especially for NAO^- events. This is because the NAO^- itself is the blocking circulation in the North Atlantic region. However, due to the fast mobility of blocking and the averaging of time and space, the percentage of IB frequency during NAO^- is not as high as we expected. Nonetheless, this is sufficient to explain the inseparable spatiotemporal connection between the NAO and blocking.

As noted by some investigators, the blocking anticyclonic circulation affects temperature advection mainly in the outer region of the blocking, and near-surface temperature through the surface radiation budget mainly in the central part of the blocking (Pfahl and Wernli, 2012). As a result, the different spatial pattern of the IB frequency distribution in the Euro-Atlantic sector due to the modulation by NAO events can affect the climate over continental Europe.

In the next section, to understand the relationship between the temperature and precipitation anomalies over Europe and their link with the IB frequency pattern, we present composites of temperature and precipitation anomalies during the different stages of the NAO life cycle.

4. Composite temperature and precipitation anomalies over Europe associated with NAO events

4.1. *Composite temperature anomalies in different stages of NAO events*

According to the composite daily NAO indices in Figs. 1b and c, the composite SAT anomalies over continental Europe are shown in Figs. 3a and b for the different stages of NAO^+ and NAO^- events. Interestingly, for the NAO^+ event (Fig. 3a), the dominant positive SAT anomaly (stippling indicates values above the 95% confidence level) is distributed along the SW–NE direction from western Europe to northeastern Europe from B1 to A1, and decays during A2, which matches the NAO^+-related blocking frequency distribution. The strongest positive SAT anomaly is in the A1 phase (decaying stage). For the NAO^- event in Fig. 3b, the negative SAT anomaly is enhanced with the increased frequency of the GB and extends from western Europe to central and northern Europe from B1 to A1, which is statistically significant (stippled region). The strongest negative SAT anomaly also occurs in the A1 phase (decaying stage). This result has not been reported previously, even though some studies have revealed that negative phases of the NAO bring colder temperatures to northern Europe and Asia, and warmer temperatures to the Mediterranean region (Kenyon and Hegerl, 2008, 2010). Thus, the strongest SAT anomaly exhibits a distinct delay relative to the strongest amplitude of the NAO event for its two phases. This may be attributable to the delay of the SAT increase/decrease due to the advection of warm/cold air (moisture) on the upstream/downstream side of the blocking anticyclone and the change in radiation fluxes [such as downward infrared radiation (IR), sensible and latent heat fluxes, and so on] due to the latitudinal shift of the Atlantic eddy-driven jet stream through the modulation of the NAO pattern (Woollings et al., 2010b). The contributions of different variables or processes to SAT changes are discussed in section 6.3.

Clearly, our results show that the two phases of NAO events have asymmetric impacts on SAT anomalies over Europe. Such an asymmetric impact between the positive and negative phases of the NAO on SAT has been suggested as attributable to the asymmetry of weather regimes (Cassou et al., 2004; Woollings et al., 2010a). Here, we further suggest that the asymmetric impact of NAO events between positive and negative phases is likely to be attributable to the asymmetry of their associated blocking frequency patterns.

4.2. *Composite precipitation anomalies in different stages of NAO events*

Figures 3c and d show the composites of precipitation anomalies over continental Europe during the life cycles of

NAO^+ and NAO^- events. The positive (negative) anomaly region above the 95% confidence level for a two-sided Student's *t*-test is indicated by stippling. For the NAO^+ event, the dominant positive precipitation anomaly (stippling indicates values above the 95% confidence level) is located over western and northern Europe along the SW–NE direction and peaks in the A1 stage (Fig. 3c). For the NAO^- event, the significant positive precipitation anomalies are seen to locate in southern Europe, mainly in the southwest (Fig. 3d), which is relatively strong from B1 to A1.

4.3. *Relationship between temperature and precipitation anomalies and the composite daily NAO index*

To further reveal the association between the evolutions of the SAT and precipitation anomalies and the daily NAO index, we show the correlation coefficient field of the composite daily NAO index with the SAT and precipitation anomalies in Fig. 4 for the NAO events. For the NAO^+ events, a positive correlation region can be seen along the SW–NE direction from southwestern Europe to northeastern Europe. Negative correlation is apparent along the SW–NE direction, but in the region from the Mediterranean Sea to the Black Sea (Fig. 4a). This hints that during the life cycle of NAO^+ events, a strong positive SAT anomaly occurs mostly over the region from western Europe to northern Europe, in agreement with the findings from Fig. 3a. The correlation field of the composite daily NAO^- index with the SAT anomaly exhibits a positive correlation distribution from western and central Europe to eastern Europe (Fig. 4a), which is a wider region (stippling indicates values above the 95% confidence level) than for the NAO^+ event in Fig. 4a. This may be because the adjustment of the negative phase circulation is more obvious, and the associated temperature change is clearer.

Also apparent from Fig. 4c is that, for the NAO^+ event, the strongest positive correlation of the precipitation anomaly with the composite daily NAO index is along the SW–NE direction, mainly in northwestern Europe, whereas the strongest negative correlation is mainly in southern Europe and some parts of central Europe. For the NAO^- event (Fig. 4d), the strongest negative correlation is concentrated in southwestern Europe. This confirms that our findings presented in Fig. 3 are statistically significant. However, the lead–lag relationship of the NAO and IB with the SAT and precipitation change is not clear. In the next section, we examine the evolution of the blocking frequency over Europe and its linkage with the life cycles of NAO events to understand the possible cause of European climate variability.

5. Evolution of blocking frequency over Europe and its linkage with temperature and precipitation anomaly changes

5.1. *Spatiotemporal connection of blocking frequency to the life cycle of NAO events*

The NAO dipole anomaly has two opposite centers, in the latitudinal bands of 60°–75°N and 35°–50°N, according to previous studies (Benedict et al., 2004; Yao and Luo, 2015). To observe the relationship between the European blocking frequency and the NAO anomaly, it is reasonable to subdivide continental Europe into two sub-regions: northern Europe (60°–75°N, 10°W–30°E) and southern Europe (35°–50°N, 10°W–30°E).

We show the time series of normalized IB frequency over northern and southern Europe in Figs. 5a and b for the different stages of NAO^+ and NAO^- events. Clearly, the NAO^+ event IB frequency over northern Europe exhibits an opposite correlation of −0.63 with the daily NAO^+ index and tends to decrease over northern Europe (blue line) during the NAO growing stage and increase during the NAO^+ decaying stage (Fig. 5a), with the opposite being the case over southern Europe (green line). The blocking frequency over southern Europe has a positive correlation of 0.93 with the daily NAO^+ index at a one-day lag. However, for the NAO^- event the blocking frequency over northern Europe exhibits a negative correlation of −0.92 with the NAO^- index at a two-day lead, which is enhanced over northern Europe during the NAO^- growing stage but reduced during the NAO^- decaying stage (Fig. 5b). It has a positive correlation of 0.95 with the daily NAO^- index over southern Europe (all correlation coefficients pass the 99% confidence test). This is consistent with the result of Scherrer et al. (2006), who noted that there is an enhanced blocking frequency over southern (northern) Europe for the positive (negative) NAO phase. However, here we present a new finding that, for the NAO^- phase, the increasing of the blocking frequency over northern Europe is a slow process, but its decline is rapid. An opposite result is found over southern Europe for the NAO^+ phase (Fig. 5a).

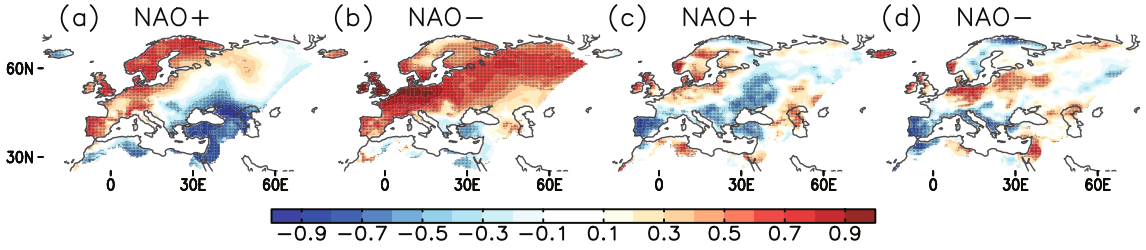

Fig. 4. Correlation distribution of the composite daily NAO indices with the (a, b) temperature and (c, d) precipitation anomalies for (a, c) NAO^+ and (b, d) NAO^- events. The stippling in all panels indicates correlation coefficients significant above the 95% confidence level for a hypothesis test.

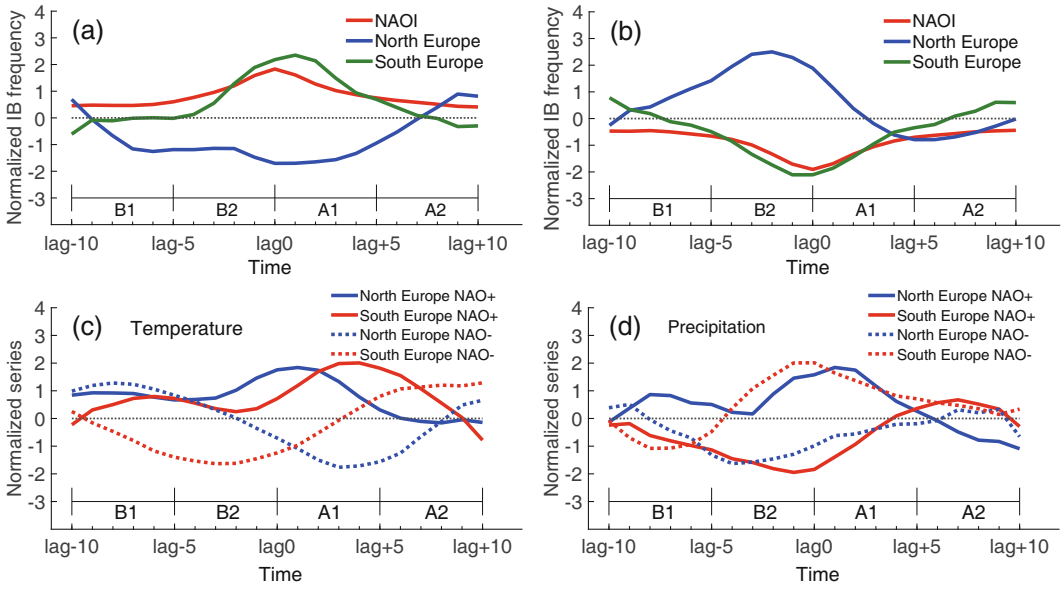

Fig. 5. (a, b) Normalized time series of IB frequency averaged over northern Europe in blue (60°–75°N, 10°W–30°E) and southern Europe in green (35°–50°N, 10°W–30°E), for (a) NAO^+ and (b) NAO^- events. The red lines represent the composite NAO index. (c, d) Normalized time series of (c) SAT and (d) precipitation averaged over northern Europe in blue (60°–75°N, 10°W–30°E) and southern Europe in red (35°–50°N, 10°W–30°E), for NAO^+ (solid line) and NAO^- (dashed line) events.

This result also indicates that the blocking frequency over northern (southern) Europe leads (lags) the evolution of the NAO^- (NAO^+) amplitude, which is consistent with the results of Yao and Luo (2015). Such a relationship can be explained in terms of the zonal movement of the NAO^- (NAO^+) dipole anomaly associated with the change in the blocking frequency, which is presented in the next section.

5.2. *Relationship between temperature and precipitation anomalies and the blocking frequency over Europe*

To further understand the association between the change in SAT and precipitation anomalies with the blocking frequency, the time series of the SAT and precipitation anomalies over northern and southern Europe are shown in Figs. 5c and d for the NAO^+ and NAO^- events. The threshold correlation coefficient of 0.56 is statistically significant at the 99% confidence level for the NAO events. Figure 5c indicates that, for the NAO^+ events (solid lines), the SAT anomaly over northern Europe exhibits a negative (positive) correlation of −0.66 (0.76) with the blocking frequency over northern (southern) Europe, but the southern Europe SAT anomaly has a negative (positive) correlation of −0.78 (0.79) with the IB frequency over northern (southern) Europe at a two-day (three-day) lag. Thus, for the NAO^+ events, when the blocking frequency is reduced over northern Europe, the positive SAT anomaly is augmented over northern Europe. For the NAO^- event (dashed lines in Fig. 5c), the SAT anomaly over northern Europe tends to have a negative correlation of −0.61 with the blocking frequency over northern Europe at a five-day lag, but a positive correlation of 0.65 over southern Europe at a four-day lag. Thus, the decline of the SAT, especially over northern Europe, lags the enhanced blocking frequency over Europe. Moreover, the decline (increase) of the SAT anomaly over Europe can be modulated by the enhancement (reduction) of the blocking frequency related to the phase of the NAO.

We can see from Fig. 5d that, for the NAO^+ event, the precipitation anomaly over northern Europe almost has an in-phase negative (positive) correlation of −0.72 (0.75) with the IB frequency over northern (southern) Europe. However, for the NAO^- event, the precipitation anomaly over southern Europe exhibits a negative correlation of −0.74 with the IB frequency over southern Europe, but a positive correlation of 0.59 with the IB frequency at a three-day lag. Thus, a comparison with Fig. 5c shows that the advent of the maximum precipitation anomaly over Europe generally precedes the maximum SAT anomaly during the NAO life cycle.

The regions of the dominant SAT and precipitation anomalies during different NAO phases can be interpreted via a sketch map of the existing region of the blocking frequency over continental Europe associated with the phase of the NAO, as shown in Fig. 6. Clearly, when the blocking frequency is distributed over Europe along the SW–NE (SE–NW) direction, the advection of warm (cold) air on the west (east) side of the blocking region leads to the increase (decrease) in the temperature anomaly over northern Europe for NAO^+ (NAO^-) events, as shown in Fig. 6a (6b). Since the warm and wet (dry and cold) air that moves along the SW–NE (NW–SE) direction inevitably encounters cold and dry (warm and wet) air on the north (south) side of Europe for the NAO^+ (NAO^-) events, the dominant positive precipitation anomaly is mainly located in northern (southern) Europe during the NAO^+ (NAO^-) episodes. Thus, it is inevitable that we observe an asymmetric impact of the NAO's phase

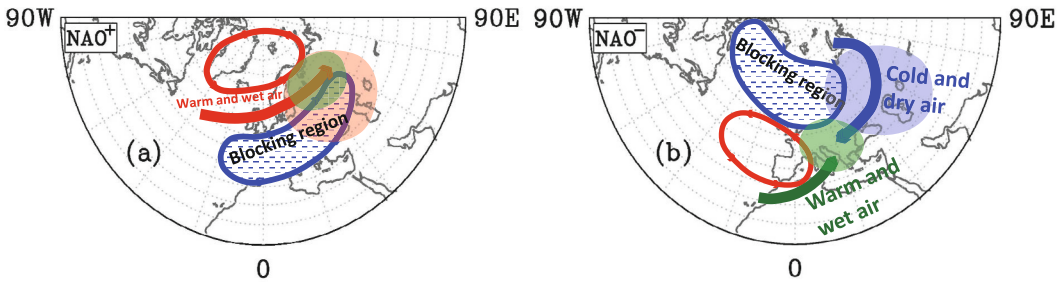

Fig. 6. Sketch map of the relationship between the blocking distribution associated with (a) NAO^+ and (b) NAO^- events and the temperature and precipitation anomalies over Europe. The red/blue shading in (a)/(b) represents the positive/negative temperature anomaly region; the positive precipitation anomaly is marked by green shading.

on the SAT and precipitation anomalies over Europe because of the different spatial distribution of the blocking frequency during the different phases of the NAO. These results have the potential to be applied in the short-term prediction of (extreme) temperature and precipitation anomalies over Europe. In addition, an approximation method is used to estimate the quantitative contribution of the IB frequency to the SAT and precipitation anomalies during an NAO event. The NAO^+ (NAO^-) events are classified into high-IB and low-IB events according to the mean IB frequency over southern (northern) Europe for all the NAO^+ (NAO^-) events. Here, the NAO^+ events with high IB frequency over southern Europe are called NAO^+-IB^+ events, and likewise for other events. Accordingly, the composite SAT and precipitation anomalies for NAO^+-IB^+ and NAO^+-IB^- (NAO^--IB^+ and NAO^--IB^-) events can be obtained, respectively. The contributions of these events to the SAT and precipitation anomalies during days lag(−10) to lag(+10) can be calculated, the results of which are shown in Table 2. The terms SAT_n and SAT_s (Pre_n and Pre_s) represent the SAT (precipitation) anomaly over northern and southern Europe, respectively. The NAO^+-IB^+ events (51 of 97 cases) account for 70%, 78%, 86% and 75% of the total SAT_n, SAT_s, Pre_n and Pre_s during NAO^+ events, respectively. The NAO^--IB^+ events (45 of 99 cases), meanwhile, account for 69%, 93%, 82% and 66% of the total SAT_n, SAT_s, Pre_n and Pre_s during NAO^- events, respectively. It can be concluded that the IB frequency during the NAO life cycle accounts for most of the contribution to the NAO total SAT and precipitation anomalies.

Table 2. Contribution of the IB frequency to SAT and precipitation (Pre) during NAO events. An NAO^+-IB^+ (NAO^+-IB^-) event represents an NAO^+ event with higher (lower) IB frequency over southern Europe than the mean value of all NAO^+ events. An NAO^--IB^+ (NAO^--IB^-) event represents an NAO^- event with higher (lower) IB frequency over northern Europe than the mean value of all NAO^- events. SAT_n (Pre_n) and SAT_s (Pre_s) mean the SAT (Pre) over northern and southern Europe, respectively.

	Classification			
	NAO^+-IB^+	NAO^+-IB^-	NAO^--IB^+	NAO^--IB^-
Number of cases	51	46	45	54
SAT_n	70%	30%	69%	31%
SAT_s	78%	22%	93%	7%
Pre_n	86%	14%	82%	18%
Pre_s	75%	25%	66%	34%

6. Possible mechanism of blocking frequency evolution during the NAO life cycle

6.1. *Blocking frequency in the Euro-Atlantic sector and its relationship with the NAO dipole anomaly and zonal wind*

To understand the physical cause of the evolution of the blocking frequency over northern and southern Europe with the NAO index, we produce a composite of 500-hPa geopotential height anomalies averaged for the four sub-periods of the NAO^+ and NAO^- events, as shown in Figs. 7a and b. It is evident in Fig. 7a (Fig. 7b) that the composite height anomaly has a negative-over-positive (positive-over-negative) dipole anomaly for the NAO^+ (NAO^-) event. With the intensification of the NAO^+ pattern the dipole height anomaly in the Atlantic sector is shifted eastward and extends into Europe, thus leading to the increased (decreased) blocking frequency over southern (northern) Europe (Fig. 7a). For the NAO^- event (Fig. 7b), the positive (negative) anomaly is mainly located in the 60°–75°N (35°–50°N) latitudinal band. Thus, it is inevitable that we observe an enhanced (reduced) blocking frequency over the North Atlantic and northern Europe (southern Europe) due to the westward shift of the dipole NAO^- anomaly from continental Europe. Thus, the evolution of the NAO event is in phase and the frequency seems able to affect the spatiotemporal changes in temperature and precipitation anomalies through altering the spatial distribution of the blocking frequency over continental Europe.

As the key analysis method used in this study, we divide an NAO event into four sub-periods and examine its spatiotemporal connection with IB, SAT and precipitation in each sub-period. However, the dynamic mechanism underpinning this connection deserves further discussion, especially the link between the NAO dipole and IB. As indicated by many studies (Luo et al., 2007, 2015a; Woollings et al., 2010b), the NAO and blocking circulation are the di-

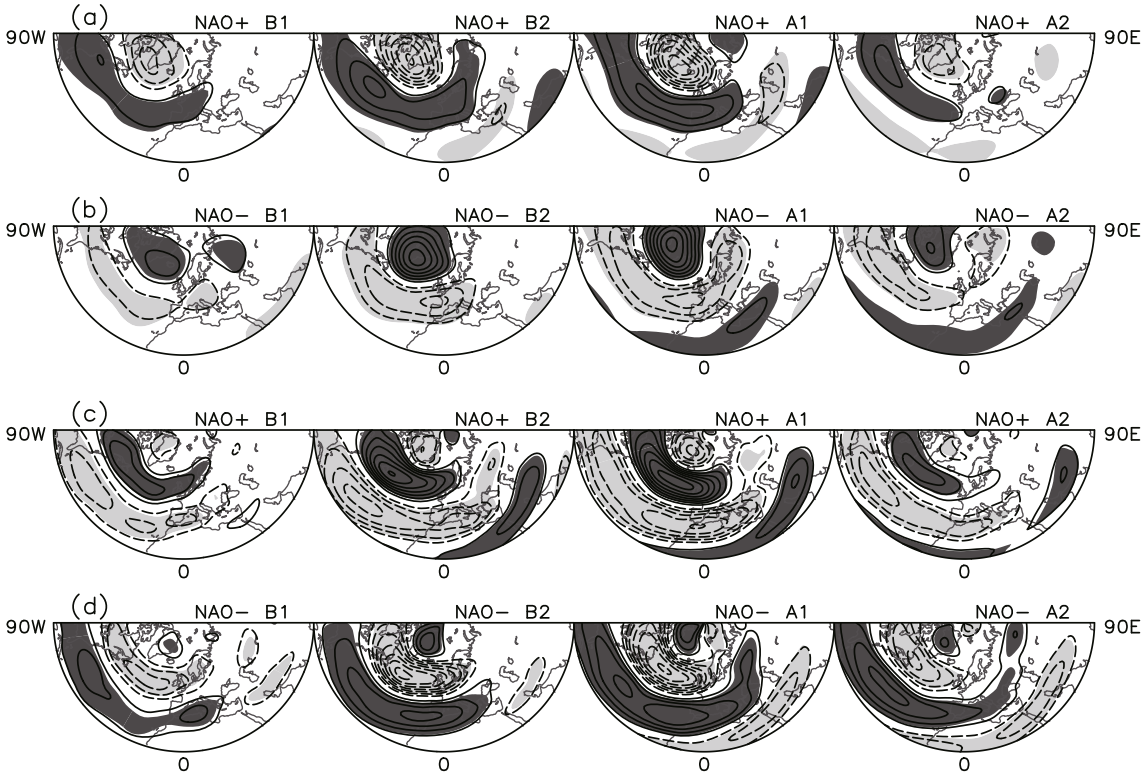

Fig. 7. Geographical distribution of composite (a, b) 500-hPa geopotential height and (c, d) 300-hPa zonal wind anomalies averaged for four sub-periods of (a, c) NAO^+ events and (b, d) NAO^- events. Dark (light) shading denotes values of positive (negative) anomalies above the 95% confidence level for a two-sided Student's *t*-test. Contours are drawn at intervals of 30 gpm in (a, b) and 2 m s^{-1} in (c, d). The lines of latitude are plotted at 5° intervals starting at 20°N.

rect manifestation of the westerly jet (zonal wind jet) changing. Accordingly, Figs. 7c and d show the composite 300-hPa zonal wind evolution during the different stages of the NAO life cycle. The 300-hPa zonal wind data are used here, instead of 500-hPa data, because the zonal wind jet core is at about the 300-hPa level, which can react more directly to the variation of the westerly jet. In addition, previous studies (Luo et al., 2015a) have also shown that results based on the 300-hPa and 500-hPa westerly wind are very consistent, because the NAO and blocking circulation are deep systems. Figure 7c shows that the zonal wind anomaly exhibits a quadrupole anomaly center over the North Atlantic–Europe region, whereas a positive center can be seen in eastern Europe. The strongest anomaly appears in the B2 and A1 stages, as the two phases are closest to lag(0). A strengthened negative anomaly can be seen at low latitudes in the North Atlantic–Europe region along the SW–NE direction. In general, a weakened zonal wind may favor the development of meridional circulation such as blocking. Therefore, it is understandable that the IB frequency center can be observed from the eastern Atlantic to northeastern Europe along the SW–NE direction, as shown in Fig. 2a. For the NAO^- event (Fig. 7d), a quadrupole anomaly distribution can also be observed over the North Atlantic–Europe region. A notable negative anomaly center can be seen over mid–high latitudes of the North Atlantic, which is consistent with the IB frequency distribution in Fig. 2b. Thus, the spatiotemporal connection between the NAO dipole and IB frequency is mainly controlled by the change in the zonal wind jet. In addition, there is also complicated nonlinear feedback and a self-maintaining mechanism between the NAO or blocking and the westerly wind, which is discussed in section 6.3.

6.2. *Zonal migration of the NAO dipole anomaly during its life cycle*

As revealed in the above subsection, the zonal migration of the NAO dipole anomaly is important for the evolution of the blocking frequency in the different regions of continental Europe during the NAO life cycle. First, meridional averaging is applied to the geopotential anomaly for the NAO life cycle over low (30°–50°N) and high (55°–75°N) latitudes, because the dominant NAO dipole anomalies are located in these two latitudinal bands. Then, the maximum and minimum position for the NAO^+ and NAO^- dipole can be identified for each day during the NAO life cycle. Figure 8 shows the zonal position of the NAO dipole during its life cycle. From Fig. 8a, the low-latitude positive anomaly center (red markers) exhibits a slight eastward shift (quasi-stationary) from day lag(−8) to lag(+2). The higher latitude negative anomaly center (blue markers) shows a quasi-stationary characteristic from day lag(−10) to lag(+10). As shown in Fig. 8b, the higher latitude positive anomaly center (red markers)

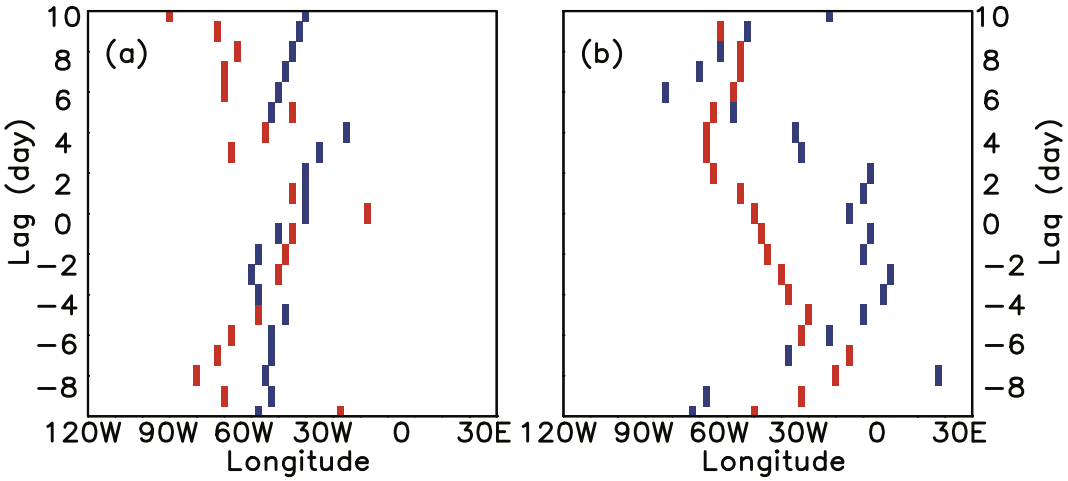

Fig. 8. Trajectory tracking of the composite daily geopotential height dipole anomalies in winter during the life cycles of (a) NAO^+ events and (b) NAO^- events. The red (blue) markers indicate the maximum (minimum) anomaly position for a positive (negative) anomaly center for the NAO dipole.

exhibits an obvious westward shift from lag(−8) to lag(+4). Meanwhile, the lower latitude anomaly center (blue markers) shows a dispersed and jumpy feature during the life cycle of NAO^-. This is because, for the NAO dipole, the anomaly center at higher latitude (negative center for NAO^+ and positive center for NAO^-), has a more concentrated distribution, which can also be seen in Figs. 7a and b. Also, the lower latitude (southern) center has a wider longitudinal range and always has multiple centers, as revealed in Yao and Luo (2014). However, the zonal migration of the NAO dipole is clearly shown in Fig. 8. At the peak day [lag(0)], the positive centers for NAO^+ and NAO^- are located near 45°W. The zonal migration of the NAO dipole may explain why the SAT and precipitation exhibit a lead–lag relationship with the NAO life cycle in different regions. The IB in Europe that leads the NAO^- can instigate cooling in southern Europe, as shown in Fig. 5c. When the NAO^- dipole undergoes a westward shift, the cold air may affect northern Europe and the SAT can exhibit an approximate three-day lag relationship with NAO^-. For the NAO^+ dipole, the eastward shift may cause the southern Europe SAT to have an approximate four-day lag relationship with NAO^+. Thus, the lead–lag relationship between the NAO and IB as revealed in Yao and Luo (2015) is important for European SAT and precipitation change in this study. Our result can be interpreted in terms of the self-maintaining mechanism of the longitudinal migration of the NAO dipole pattern, proposed in the next subsection.

6.3. *Physical mechanism of NAO migration*

The NAO's circulation is controlled by the background westerly wind. To examine the physical mechanism of the shift in the NAO, Fig. 9 shows the 300-hPa zonal wind distribution and its latitudinal profile in the Atlantic–Europe region. Clearly, the zonal wind anomaly exhibits a wave train distribution along the north–south direction. The single midlatitude strong wind jet for NAO^+ in Fig. 9a and double-branch jet for NAO^- in Fig. 9b are clear to see. The strong midlatitude jet is conducive to the eastward migration of the NAO^+ dipole, while the negative anomaly center at midlatitudes favors the westward migration of the NAO^- dipole. To be specific, the migration mechanism of the NAO dipole can be explained by the wind profile in Fig. 9. The wind over northern Europe (dashed line in Fig. 9b; 50°–70°N) is weak and the positive anomaly may undergo westward movement. The strengthening of the wind over the low (20°–40°N) and high (65°–80°N) latitude Atlantic is due to the feedback of the NAO^- circulation development. For NAO^+ events (Fig. 9a), as the NAO^+ dipole grows in the Atlantic region, the zonal wind is intensified at midlatitudes (40°–60°N). The strong wind jet may drive the NAO^+ dipole to move toward continental Europe. Due to the feedback of NAO^+ development, the zonal wind jet in Europe may shift northward, as shown in Fig. 9a (dashed line). This is called the self-maintaining mechanism of the NAO, as revealed in Luo et al. (2007) and Yao and Luo (2015). This mechanism can be used here to explain the lead–lag relationship of the NAO and IB with the SAT and precipitation.

Many studies have suggested that RWB follows the horizontal gradient of the basic zonal wind (Thorncroft et al., 1993; Tyrlis and Hoskins, 2008a, b). An NAO^- (GB) event preceded by a blocking event over northern Europe can be explained by the wave breaking viewpoint of Woollings et al. (2008). This is because the cyclonic wave breaking over Greenland leading to an NAO^- event can arise from the cyclonic shear of the Atlantic jet due to the southward displacement of the jet core. The southward shift of the jet core may be caused by the retrogression of the European blocking. However, during NAO^+ events the anticyclonic (rotation) wave breaking on the equatorward side of the jet does not allow this retrogression, instead leading to the eastward migration of the NAO^+ dipole pattern. Thus, as shown in Fig. 9a, when the Atlantic jet is shifted northward, the NAO^+

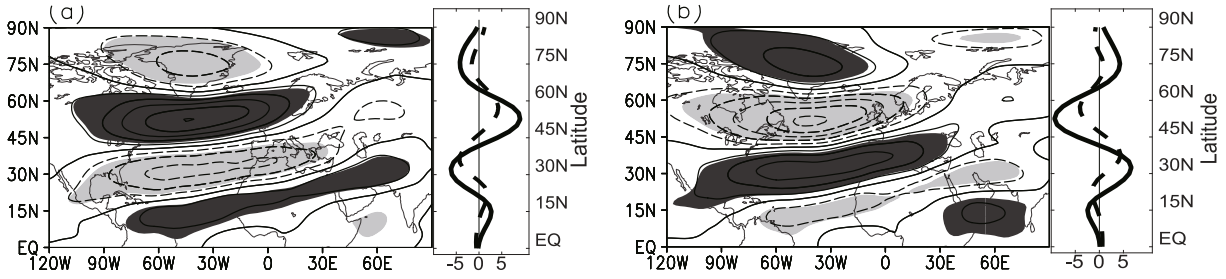

Fig. 9. Spatial distribution and latitudinal profile of time-mean 300-hPa zonal winds from lag(−10) to lag(+10) averaged for (a) NAO^+ events and (b) NAO^- events. Units: m s^{-1}. Dark (light) shading denotes regions of positive (negative) anomalies above the 95% confidence level for a two-sided Student's *t*-test. Contours are drawn at intervals of 2 m s^{-1}. The solid (dashed) line in the right-hand part of each panel represents the zonal wind profile averaged over the Atlantic basin (Europe) for the region 60°–10°W (10°W–60°E).

dipole pattern associated with the anticyclonic wave breaking precedes the genesis of European blocking events. This provides a dynamical explanation as to why there is a lead–lag relationship between SAT or precipitation and the NAO. However, to keep the length of this paper to an acceptable limit, we do not provide a specific quantitative analysis of why there is a three- or four-day lead–lag relationship between SAT and the NAO. As revealed in Yao and Luo (2015), the lead–lag relationship between the NAO dipole and instantaneous European blocking is important, and in this study we further examine the meteorological (SAT and precipitation) impact caused by this lead–lag relationship.

6.4. *Contribution of radiative fluxes to the SAT anomaly*

In order to examine the primary factor determining the variability of the SAT anomaly ($\partial_t T$), it is necessary to quantify the surface radiation ($\partial_t T_{\mathrm{IR}}$), heat flux ($\partial_t T_{\mathrm{SL}}$) and temperature advection ($\partial_t T_{\mathrm{advection}}$) and adiabatic ($\partial_t T_{\mathrm{adibatic}}$) terms. Here, the units of the above variables are all unified into W m^{-2}, following previous work (Alexeev et al., 2005; Yao et al., 2017). In addition, the cloud forcing net solar flux at the surface and the precipitable water for the entire atmosphere are also examined to clarify in detail their respective contributions to the SAT anomaly.

Figure 10a shows the composite of the surface downward IR anomaly for the four sub-periods of the NAO^+ and NAO^- events. It is apparent that, for NAO^+ events (Fig. 10a, top), the downward IR exhibits a large positive anomaly (stippling indicates values above the 95% confidence level) over northern Europe along the SW–NE direction. The positive anomaly develops strongest in the A1 stage, which is consistent with the SAT results in Fig. 3a. A negative anomaly is seen in southeastern Europe in Fig. 10a (top), which has a wider area compared with Fig. 3a. This is because the radiation data used for Fig. 10 are from the NCEP–NCAR reanalysis dataset, which covers the ocean and land region. The SAT and precipitation data only cover the land area. For NAO^- events (Fig. 10a, bottom), the distribution is opposite and exhibits asymmetry compared with NAO^+ (Fig. 10a, top). The strongest negative anomaly with significant values (stippling) can also be seen in the A1 stage. Overall, the downward IR makes an important contribution to the enhancement (decline) of the positive (negative) SAT anomaly during the NAO life cycle.

The composite sensible and latent heat fluxes are shown in Fig. 10b. Clearly, the sensible and latent heat fluxes over the ocean region are relatively stronger than over the land region. This is because the interaction between water and air is stronger and more complicated than that over land. Over continental Europe, the sensible and latent heat fluxes can make a considerable contribution to the enhancement of the SAT anomaly during the NAO^+ life cycle, especially in the B1 and A1 stages (Fig. 10b, top). Meanwhile, the negative sensible and latent heat anomaly over continental Europe during the NAO^- life cycle is also significant in the B2 and A1 stages (Fig. 10b, bottom). This indicates that the sensible and latent heat flux can also make a certain contribution to the SAT anomaly. However, the pattern of sensible and latent heat fluxes shows local and spatial discontinuities (Fig. 10b), which is different to the pattern of IR and SAT.

Figure 10c shows the composite 850-hPa horizontal temperature advection for NAO^+ and NAO^- events. The positive and negative anomaly patterns (stippling for those above the 95% confidence level) of temperature advection bear some similarity to the SAT pattern. However, it can be seen that the temperature advection over land is weaker compared with the downward IR and sensible and latent heat fluxes. Figure 10d shows the adiabatic term ($\partial_t T_{\mathrm{adibatic}}$) caused by the vertical velocity anomaly, from which it can be concluded that the magnitude of the adiabatic heating and cooling is very small compared to that of the other terms, as indicated in Yao et al. (2017). Moreover, the composite cloud forcing net solar flux at the surface for NAO^+ and NAO^- events is also shown in Fig. 10e. It can be seen that the cloud forcing net solar flux at the surface makes an opposite contribution to the SAT anomaly, with a smaller magnitude, especially in stages A1 and A2. It also shows a transition from positive to negative over continental Europe for NAO^+ events. This may be caused by the establishment of NAO circulation and cloud formation. Figure 10f further shows the composite precipitable water for the entire atmosphere for NAO events. It can be seen that the pattern of precipitable water is remarkably

consistent with the IR and SAT patterns. Among which (Fig. 10f, top), the positive water vapor exhibits a marked (statistically significant) SW–NE distribution, reaching a peak in B2, and vice versa for NAO$^-$ events (Fig. 10f, bottom). The peak stage for water vapor is earlier than that for IR and SAT, which may be due to the process of cloud formation by water vapor, and this will be examined in future research. It has been revealed that the downward IR is closely related to lower-tropospheric water vapor content and temperature (Zhang et al., 1995), which plays a crucial role in affecting SAT variability. According to Gong et al. (2017) and Luo et al. (2017), the NAO and blocking circulation play a major role in the transportation of water vapor.

Upon comparison of Figs. 10a–f, it can be concluded that IR makes a more important contribution to controlling the SAT over Europe during the NAO life cycle by regulating the

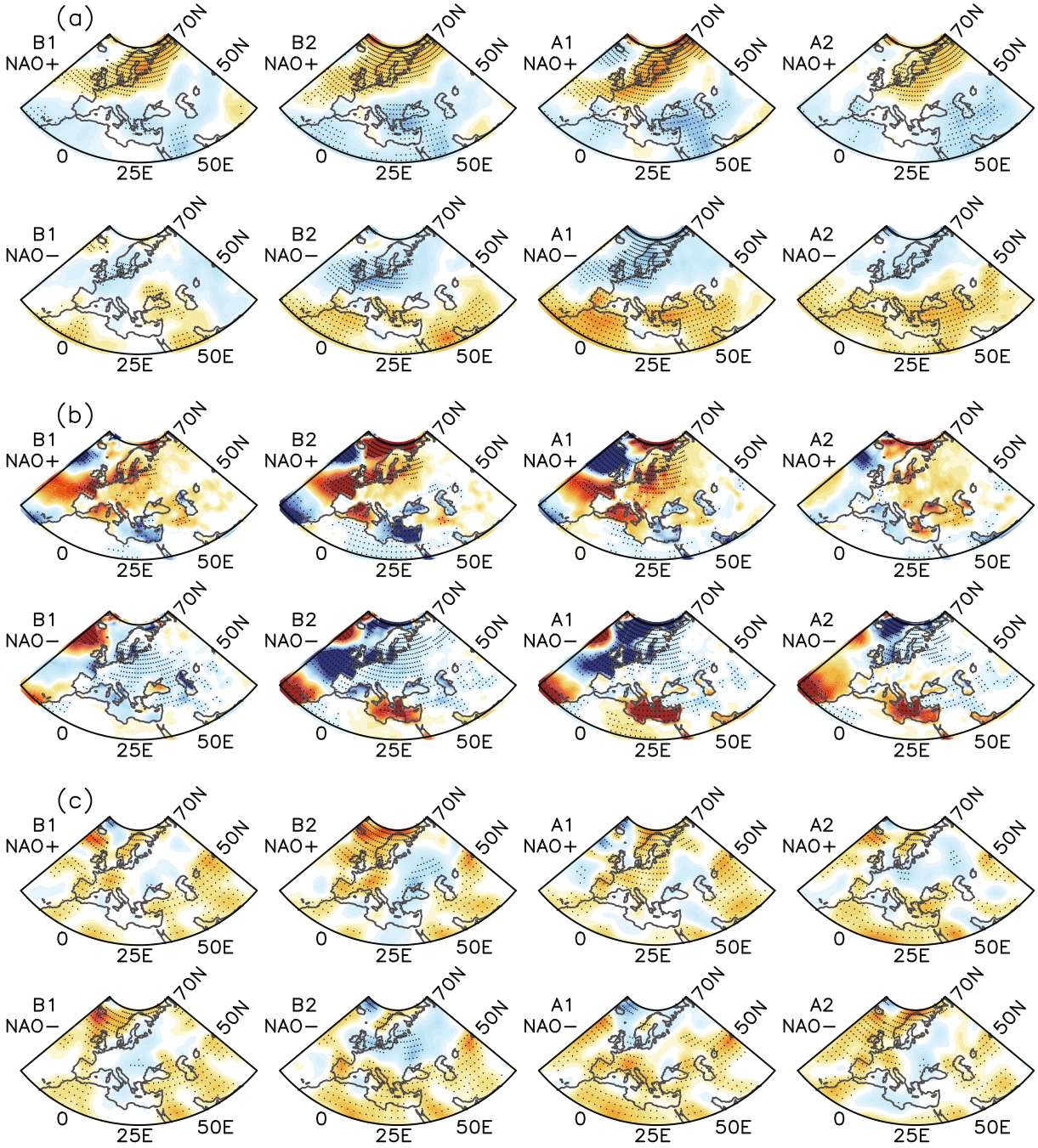

Fig. 10. Geographical distribution of the composite (a) surface downward IR anomaly, (b) sum of surface sensible and latent heat flux anomaly, (c) 850-hPa horizontal temperature advection anomaly, (d) adiabatic heating/cooling induced by vertical velocity anomaly, (e) cloud forcing net solar flux at the surface anomaly, and (f) precipitable water anomaly, averaged for four sub-periods of NAO$^+$ events and NAO$^-$ events. Stippling indicates values above the 95% confidence level for a two-sided Student's *t*-test. The units are W m^{-2} in (a–e) and kg m^{-2} in (f).

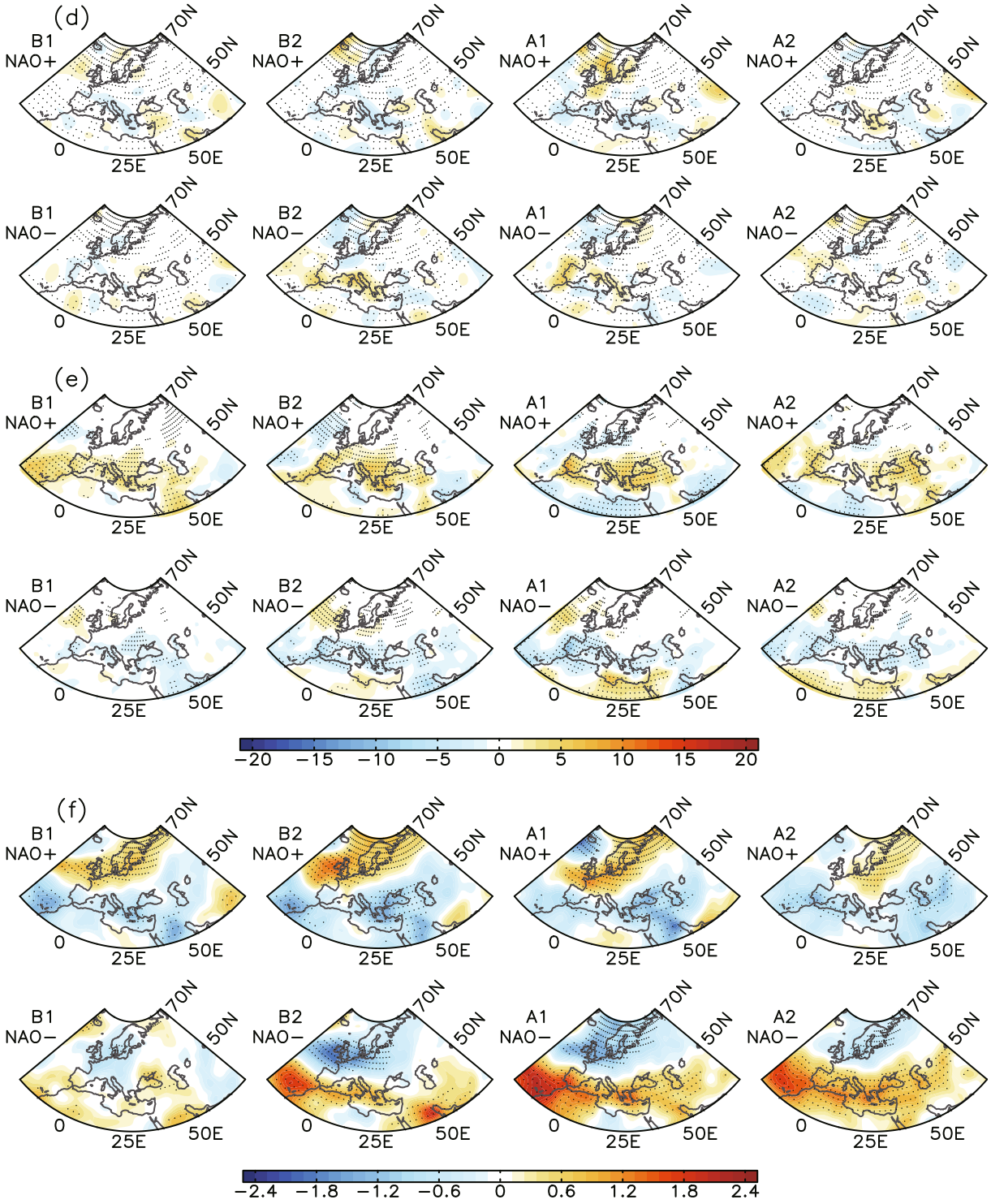

Fig. 10. (Continued.)

distribution of water vapor. Meanwhile, the SAT anomaly is also affected by temperature advection, surface sensible and latent heat fluxes, and other radiative fluxes (e.g., cloud forcing net solar flux). Interestingly, the precipitation distribution (Figs. 3c and d) is similar to the downward IR pattern (Fig. 10a) and the water vapor pattern (Fig. 10f). This may contribute to the water vapor transport via the NAO's circulation, which is conducive to the strengthening of precipitation.

7. Discussion and conclusions

This paper examines the asymmetric spatiotemporal evolution of Euro-Atlantic blocking during the NAO life cycle and the possible physical cause of the genesis of a winter

asymmetric weather impact over Europe. It is found that the spatial pattern of the blocking frequency in the Euro-Atlantic sector is dominated by the phase of the NAO during its entire life cycle. The higher blocking frequency for the NAO^+ phase is distributed along the SW–NE direction, while the blocking events exhibit an enhanced frequency along the SE–NW direction for the NAO^- phase. An asymmetric spatial connection between NAO phases and blocking is seen here. Thus, a negative (positive) correlation is seen between the NAO and blocking over the North Atlantic and northern Europe (eastern Atlantic and southern Europe). This suggests that there is an enhanced (reduced) blocking frequency over northern (southern) Europe during NAO^- events, with an opposite variation of the blocking frequency for NAO^+ events. This result is supplemental to those reported in previous studies (Scherrer et al., 2006; Croci-Maspoli et al., 2007; Luo et al., 2007, 2015a). Moreover, the most evident blocking frequency is seen in the decaying stage for the NAO^+ phase and growing stage for the NAO^- phase. This means that the temporal evolution of the NAO and blocking has an asymmetric connection. Thus, the phase of the NAO seems to determine the latitudinal and longitudinal change of the blocking frequency in the continental areas of the Euro-Atlantic sector.

Because warm (cold) temperature and moisture advection prevails on the west (east) side of the blocking circulation, the phase of the NAO can affect the temperature anomaly over continental Europe through modulating the spatial distribution of the blocking frequency. The significant positive (negative) temperature anomaly over Europe is dominated by the SW–NE-oriented (SE–NW-oriented) distribution of the blocking frequency in the Euro-Atlantic sector. A new finding is that the most obvious increase (decline) in the temperature anomaly over Europe takes place in the decaying stage of the positive (negative) NAO phase due to the delaying effect of the temperature and moisture advection along the west (east) side of the blocking anticyclone. On the other hand, we can see that positive precipitation anomalies occur over northern (southern) Europe in positive (negative) NAO phases. In addition, it is found that the downward IR modulated by the NAO's circulation makes a more important contribution to the SAT change, as compared with sensible and latent heat fluxes and horizontal temperature advection.

Finally, a physical explanation as to why the blocking frequency is enhanced over northern (southern) Europe during negative (positive) NAO phases is provided based on composite analysis. It is found that enhanced blocking frequency over northern (southern) Europe is closely related to the westward (eastward) migration of the NAO^- (NAO^+) dipole anomaly. Moreover, it is further shown that the westward (eastward) shift of the NAO^- (NAO^+) dipole anomaly is attributable to the strengthening (weakening) of zonal winds in mid–high latitude regions during positive (negative) NAO phases, which is considered as a self-maintaining phenomenon of the NAO's occurrence. Thus, the lead–lag (asymmetric) relationship between the NAO and blocking, associated with SAT and precipitation changes, is due to the NAO self-maintaining mechanism.

It must, however, be pointed out that this paper does not reveal the physical reason why the NAO or blocking dipole centers are not located at the same longitude and exhibit asymmetric features (zonal tilt of the segment line for north–south dipole centers) during the life cycle. Further investigations are needed.

Acknowledgements. The authors acknowledge support from the National Natural Science Foundation of China (Grant Nos. 41505075 and 41790473) and the National Key Research and Development Program of China (Grant No. 2016YFA0601802). The authors also acknowledge the E-OBS dataset from the EU-FP6 project ENSEMBLES (http://ensembles-eu.metoffice.com) and the data providers in the ECA&D project (http://www.ecad.eu).

REFERENCES

Alexander, L. V., and Coauthors, 2006: Global observed changes in daily climate extremes of temperature and precipitation. *J. Geophys. Res*., **111**, https://doi.org/10.1029/2005JD006290.

Alexeev, V. A., P. L. Langen, and J. R. Bates, 2005: Polar amplification of surface warming on an aquaplanet in "ghost forcing" experiments without sea ice feedbacks. *Climate Dyn*., **24**, 655–666, https://doi.org/10.1007/s00382-005-0018-3.

Barnston, A. G., and R. E. Livezey, 1987: Classification, seasonality and persistence of low-frequency atmospheric circulation patterns. *Mon. Wea. Rev*., **115**, 1083–1126, https://doi.org/10.1175/1520-0493(1987)115<1083:CSAPOL>2.0.CO;2.

Benedict, J. J., S. Lee, and S. B. Feldstein, 2004: Synoptic view of the North Atlantic oscillation. *J. Atmos. Sci*., **61**, 121–144, https://doi.org/10.1175/1520-0469(2004)061<0121:SVOTNA>2.0.CO;2.

Berrisford, P., B. J. Hoskins, and E. Tyrlis, 2007: Blocking and Rossby wave breaking on the dynamical tropopause in the Southern Hemisphere. *J. Atmos. Sci*., **64**, 2881–2898, https://doi.org/10.1175/JAS3984.1.

Buehler, T., C. C. Raible, and T. F. Stocker, 2011: The relationship of winter season North Atlantic blocking frequencies to extreme cold or dry spells in the ERA-40. *Tellus A*, **63**, 174–187, https://doi.org/10.1111/j.1600-0870.2010.00492.x.

Cassou, C., L. Terray, J. W. Hurrell, and C. Deser, 2004: North Atlantic winter climate regimes: Spatial asymmetry, stationarity with time, and oceanic forcing. *J. Climate*, **17**, 1055–1068, https://doi.org/10.1175/1520-0442(2004)017<1055:NAWCRS>2.0.CO;2.

Cattiaux, J., R. Vautard, C. Cassou, P. Yiou, V. Masson-Delmotte, and F. Codron, 2010: Winter 2010 in Europe: A cold extreme in a warming climate. *Geophys. Res. Lett*., **37**, L20704, https://doi.org/10.1029/2010GL044613.

Croci-Maspoli, M., C. Schwierz, and H. C. Davies, 2007: Atmospheric blocking: Space–time links to the NAO and PNA. *Climate Dyn*., **29**, 713–725, https://doi.org/10.1007/s00382-007-0259-4.

Davini, P., C. Cagnazzo, R. Neale, and J. Tribbia, 2012a: Coupling between Greenland blocking and the North Atlantic oscillation pattern. *Geophys. Res. Lett*., **39**, L14701, https://doi.org/10.1029/2012GL052315.

Davini, P., C. Cagnazzo, S. Gualdi, and A. Navarra, 2012b: Bidimensional diagnostics, variability, and trends of Northern Hemisphere blocking. *J. Climate*, **25**, 6496–6508, https://

doi.org/10.1175/JCLI-D-12-00032.1.

Diao, Y. N., J. P. Li, and D. H. Luo, 2006: A new blocking index and its application: Blocking action in the Northern Hemisphere. *J. Climate*, **19**, 4819–4839, https://doi.org/10.1175/JCLI3886.1.

Franzke, C., S. Lee, and S. B. Feldstein, 2004: Is the North Atlantic oscillation a breaking wave? *J. Atmos. Sci*., **61**, 145–160, https://doi.org/10.1175/1520-0469(2004)061<0145:ITNAOA>2.0.CO;2.

Gong, T. T., and D. H. Luo, 2017: Ural Blocking as an amplifier of the Arctic sea ice decline in winter. *J. Climate*, **30**, 2639–2654, https://doi.org/10.1175/JCLI-D-16-0548.1.

Gong, T. T., S. B. Feldstein, and S. Lee, 2017: The role of downward infrared radiation in the recent Arctic winter warming trend. *J. Climate*, **30**, 4937–949, http://doi.org/10.1175/JCLI-D-16-0180.1.

Haylock, M. R., N. Hofstra, A. M. G. K. Tank, E. J. Klok, P. D. Jones, and M. New, 2008: A European daily high-resolution gridded data set of surface temperature and precipitation for 1950–2006. *J. Geophys. Res*., **113**, D20119, https://doi.org/10.1029/2008jd010201.

Hurrell, J. W., 1995: Decadal trends in the North Atlantic oscillations: Regional temperatures and precipitation. *Science*, **269**, 676–679, https://doi.org/10.1126/science.269.5224.676.

Hurrell, J. W., Y. Kushnir, G. Ottersen, and M. Visbeck, 2003: An overview of the North Atlantic oscillation. *The North Atlantic Oscillation: Climatic Significance and Environmental Impact*, J. W. Hurrell, Y. Kushnir, G. Ottersen, and M. Visbeck, Eds., AGU Geophysical Monograph, Vol. 134, 1–35, https://doi.org/10.1029/134GM01.

Kenyon, J., and G. C. Hegerl, 2008: Influence of modes of climate variability on global temperature extremes. *J. Climate*, **21**, 3872–3889, https://doi.org/10.1175/2008JCLI2125.1.

Kenyon, J., and G. C. Hegerl, 2010: Influence of modes of climate variability on global precipitation extremes. *J. Climate*, **23**, 6248–6262, https://doi.org/10.1175/2010JCLI3617.1.

Luo, B. H., D. H. Luo, L. X. Wu, L. H. Zhong, and I. Simmonds, 2017: Atmospheric circulation patterns which promote winter Arctic sea ice decline. *Environ. Res. Lett.*, **12**, 054017, https://doi.org/10.1088/1748-9326/aa69d0.

Luo, D. H., 2005a: Why is the North Atlantic block more frequent and long-lived during the negative NAO phase? *Geophys. Res. Lett.*, **32**, L20804, https://doi.org/10.1029/2005GL022927.

Luo, D. H., 2005b: A barotropic envelope Rossby soliton model for block-eddy interaction. Part I: Effect of topography. *J. Atmos. Sci*., **62**(1), 5–21, https://doi.org/10.1175/1186.1.

Luo, D. H., A. Lupo, and H. Wan, 2007: Dynamics of eddy-driven low-frequency dipole modes. Part I: A simple model of North Atlantic oscillations. *J. Atmos. Sci*., **64**, 3–38, https://doi.org/10.1175/JAS3818.1.

Luo, D. H., J. Cha, and S. B. Feldstein, 2012: Weather regime transitions and the interannual variability of the North Atlantic oscillation. Part I: A likely connection. *J. Atmos. Sci*., **69**, 2329–2346, https://doi.org/10.1175/JAS-D-11-0289.1.

Luo, D. H., J. Cha, L. H. Zhong, and A. G. Dai, 2014: A nonlinear multi-scale interaction model for atmospheric blocking: The eddy-blocking matching mechanism. *Quart. J. Roy. Meteor. Soc*., **140**(683), 1785–1808, https://doi.org/10.1002/qj.2337.

Luo, D. H., Y. Yao, and A. G. Dai, 2015a: Decadal relationship between European blocking and the North Atlantic oscillation during 1978-2012. Part I: Atlantic conditions. *J. Atmos. Sci*., **72**, 1152–1173, https://doi.org/10.1175/JAS-D-14-0039.1.

Luo, D. H., Y. Yao, and A. G. Dai, 2015b: Decadal relationship between European blocking and the North Atlantic oscillation during 1978–2012. Part II: A theoretical model study. *J. Atmos. Sci*., **72**, 1174–1199, https://doi.org/10.1175/JAS-D-14-0040.1.

McIntyre, M. E., and T. N. Palmer, 1983: Breaking planetary waves in the stratosphere. *Nature*, **305**, 593–600, https://doi.org/10.1038/305593a0.

Mitchell, D. M., L. J. Gray, J. Anstey, M. P. Baldwin, and A. J. Charlton-Perez, 2013: The influence of stratospheric vortex displacements and splits on surface climate. *J. Climate*, **26**, 2668–2682, https://doi.org/10.1175/JCLI-D-12-00030.1.

Nie, Y., Y. Zhang, G. Chen, X.-Q. Yang, and D. A. Burrows, 2014: Quantifying barotropic and baroclinic eddy feedbacks in the persistence of the Southern Annular Mode. *Geophys. Res. Lett*., **41**, 8636–8644, https://doi.org/10.1002/2014GL062210.

Nie, Y., Y. Zhang, G. Chen, and X. Q. Yang, 2016: Delineating the barotropic and baroclinic mechanisms in the midlatitude eddy-driven jet response to lower-tropospheric thermal forcing. *J. Atmos. Sci.*, **73**, 429–448, https://doi.org/10.1175/JAS-D-15-0090.1.

Ouzean, G., J. Cattiaux, H. Douville, A. Ribes, and D. Saint-Martin, 2011: European cold winter 2009-2010: How unusual in the instrumental record and how reproducible in the ARPEGE-climat model? *Geophys. Res. Lett.*, **38**, L11706, https://doi.org/10.1029/2011GL047667.

Pelly, J. L., and B. J. Hoskins, 2003: A new perspective on blocking. *J. Atmos. Sci*., **60**, 743–755, https://doi.org/10.1175/1520-0469(2003)060<0743:ANPOB>2.0.CO;2.

Pfahl, S., and H. Wernli, 2012: Quantifying the relevance of atmospheric blocking for co-located temperature extremes in the Northern Hemisphere on (sub-) daily time scales. *Geophys. Res. Lett*., **39**, L12807, https://doi.org/10.1029/2012gl052261.

Rivière, G., and I. Orlanski, 2007: Characteristics of the Atlantic storm-track eddy activity and its relation with the North Atlantic oscillation. *J. Atmos. Sci*., **64**, 241–266, https://doi.org/10.1175/JAS3850.1.

Scaife, A. A., C. K. Folland, L. V. Alexander, A. Moberg, and J. R. Knight, 2008: European climate extremes and the North Atlantic oscillation. *J. Climate*, **21**, 72–83, https://doi.org/10.1175/2007JCLI1631.1.

Scherrer, S., M. Croci-Maspoli, C. Schwierz, and C. Appenzeller, 2006: Two- dimensional indices of atmospheric blocking and their statistical relationship with winter climate patterns in the Euro-Atlantic region. *Int. J. Climatol*., **26**, 233–249, https://doi.org/10.1002/joc.1250.

Schwierz, C., M. Croci-Maspoli, and H. C. Davies, 2004: Perspicacious indicators of atmospheric blocking. *Geophys. Res. Lett*., **31**, L06125, https://doi.org/10.1029/2003gl019341.

Shabbar, A., J. P. Huang, and K. Higuchi, 2001: The relationship between the wintertime North Atlantic oscillation and blocking episodes in the North Atlantic. *Int. J. Climatol*., **21**, 355–369, https://doi.org/10.1002/joc.612.

Sillmann, J., and M. Croci-Maspoli, 2009: Present and future atmospheric blocking and its impact on European mean and extreme climate. *Geophys. Res. Lett.*, **36**, L10702, https://doi.org/10.1029/2009GL038259.

Sillmann, J., M. Croci-Maspoli, M. Kallache, and R. W. Katz, 2011: Extreme cold winter temperatures in Europe under the

influence of North Atlantic atmospheric blocking. *J. Climate*, **24**, 5899–5913, https://doi.org/10.1175/2011JCLI4075.1.

Simolo, C., M. Brunetti, M. Maugeri, and T. Nanni, 2011: Evolution of extreme temperatures in a warming climate. *Geophys. Res. Lett.*, **38**, L16701, https://doi.org/10.1029/2011GL048437.

Strong, C., and G. Magnusdottir, 2008: Tropospheric Rossby wave breaking and the NAO/NAM. *J. Atmos. Sci.*, **65**, 2861–2876, https://doi.org/10.1175/2008JAS2632.1.

Sung, M. K., G. H. Lim, J. S. Kug, and S. I. An, 2011: A linkage between the North Atlantic Oscillation and its downstream development due to the existence of a blocking ridge. *J. Geophys. Res.*, **116**, D11107, https://doi.org/10.1029/2010JD015006.

Thorncroft, C. D., B. J. Hoskins, and M. E. Mcintyre, 1993: Two paradigms of baroclinic-wave life-cycle behavior. *Quart. J. Roy. Meteor. Soc.*, **119**, 17–55, https://doi.org/10.1002/qj.49711950903.

Tibaldi, S., and F. Molteni, 1990: On the operational predictability of blocking. *Tellus A*, **42**, 343–365, https://doi.org/10.3402/tellusa.v42i3.11882.

Tyrlis, E., and B. J. Hoskins, 2008a: Aspects of a Northern Hemisphere atmospheric blocking climatology. *J. Atmos. Sci.*, **65**, 1638–1652, https://doi.org/10.1175/2007JAS2337.1.

Tyrlis, E., and B. J. Hoskins, 2008b: The morphology of Northern Hemisphere blocking. *J. Atmos. Sci.*, **65**, 1653–1665, https://doi.org/10.1175/2007JAS2338.1.

Walker, G. T., and E. W. Bliss, 1932: World weather. *V. Mem. Roy. Meteor. Soc.*, **4**, 53–84.

Wang, C. Z., H. L. Liu, and S. K. Lee, 2010: The record-breaking cold temperatures during the winter of 2009/2010 in the Northern Hemisphere. *Atmos. Sci. Lett.*, **11**, 161–168, https://doi.org/10.1002/asl.278.

Woollings, T., A. Hannachi, and B. Hoskins, 2010b: Variability of the North Atlantic eddy-driven jet stream. *Quart. J. Roy. Meteor. Soc.*, **136**, 856–868, https://doi.org/10.1002/qj.625.

Woollings, T., A. Hannachi, B. Hoskins, and A. Turner, 2010a: A regime view of the North Atlantic oscillation and its response to anthropogenic forcing. *J. Climate*, **23**, 1291–1307, https://doi.org/10.1175/2009JCLI3087.1.

Woollings, T., B. Hoskins, M. Blackburn, and P. Berrisford, 2008: A new Rossby wave-breaking interpretation of the North Atlantic Oscillation. *J. Atmos. Sci.*, **65**, 609–626, https://doi.org/10.1175/2007JAS2347.1.

Yao, Y., and D. H. Luo, 2014: Relationship between zonal position of the North Atlantic Oscillation and Euro-Atlantic blocking events and its possible effect on the weather over Europe. *Science China Earth Sciences*, **57**, 2628–2636, https://doi.org/10.1007/s11430-014-4949-6.

Yao, Y., and D. H. Luo, 2015: Do European blocking events precede North Atlantic Oscillation events? *Adv. Atmos. Sci.*, **32**(8), 1106–1118, https://doi.org/10.1007/s00376-015-4209-5.

Yao, Y., D. H. Luo, A. G. Dai, and I. Simmonds, 2017: Increased quasi stationarity and persistence of winter Ural blocking and Eurasian extreme cold events in response to Arctic warming. Part I: Insights from observational analyses. *J. Climate*, **30**(10), 3549–3568, https://doi.org/10.1175/JCLI-D-16-0261.1.

Zhang, Y.-C., W. B. Rossow, and A. A. Lacis, 1995: Calculation of surface and top of atmosphere radiative fluxes from physical quantities based on ISCCP data sets. 1: Method and sensitivity to input data uncertainties. *J. Geophys. Res.*, **100**, 1149–1165, https://doi.org/10.1029/94JD02747.